Investigating Mach 4 Un-Start Dynamics and Experimental Validation in a Supersonic Wind Tunnel

a project presented to

The Faculty of the Department of Aerospace Engineering

San José State University

in partial fulfillment of the requirements for the degree

Master of Science in Aerospace Engineering

by

Dan Orteza

December 2025

Approved by

Dr. Periklis Papadopoulos

Faculty Advisor



© 2025
Dan Orteza
ALL RIGHTS RESERVED

ABSTRACT

Investigating Mach 4 Un-Start Dynamics and Experimental Validation in a Supersonic Wind Tunnel

Dan Orteza

Supersonic flow at Mach 4 presents significant challenges for aerodynamic stability, propulsion system operability, and experimental repeatability. One of the most critical flow instabilities in this regime is inlet unstart, a sudden breakdown of supersonic flow caused by shock motion, boundary layer separation, and excessive backpressure. Unstart poses a major risk to both hypersonic air-breathing propulsion systems and high-speed wind tunnel testing. This project investigated Mach 4 unstart dynamics through a combined computational and experimental approach conducted at the Naval Postgraduate School Mach 4 supersonic wind tunnel.

Computational Fluid Dynamics (CFD) simulations were performed using STAR-CCM+ and ANSYS Fluent to model tunnel startup, shock formation, and injection-induced flow disturbances. Inviscid and Reynolds-averaged Navier–Stokes formulations with the SST k–ω turbulence model were employed to establish a validated Mach 4 baseline flow and to explore unstart initiation through controlled geometric blockage and secondary mass

injection. The simulations demonstrated that fixed-position mass injection and localized blockage at the second throat were capable of generating a near-normal shock and a complete unstart under sufficient disturbance magnitude.

Guided by the CFD results, an experimental campaign was conducted using a series of additively manufactured and metallic injector geometries, including multi-port nozzles and simplified pipe-based injectors. Schlieren imaging was used to visualize shock structures and flow disturbances during testing. While experimental configurations consistently produced localized compression waves and shock structures consistent with numerical predictions, a global unstart was not achieved. Structural survivability limits, injection pressure constraints, and facility operational limitations restricted the achievable disturbance levels during testing.

Despite these limitations, the study validated the numerical startup model, identified critical injector failure modes, and established the structural and flow requirements necessary for injection-driven unstart at Mach 4. The results provide a robust computational baseline, experimental insight into high-speed injection-induced disturbances, and a clear path forward for future unstart investigations using strengthened hardware and higher-capacity injection systems.

Acknowledgments

I would like to express my deepest gratitude to those who have supported and guided me throughout this project.

First and foremost, I sincerely thank my supervisor at the Naval Postgraduate School, Dr. Garth Hobson, for his invaluable mentorship and support during my time at NPS. His guidance has been instrumental in shaping the direction of this research. I also extend my appreciation to the master's students studying under him, whose insights, collaboration, and discussions have greatly contributed to my understanding and progress.

I am also immensely grateful to my primary advisor at San José State University, Dr. Periklis Papadopoulos, for his continued encouragement, expertise, and insightful feedback, which have been essential in refining my work.

I would like to give special recognition to Professor Brian Andrade, who generously dedicated countless hours advising me on how to use the Star CCM+ software and helping me refine and troubleshoot my simulation setup.

His support and patience played a critical role in the successful execution of the computational phase of this project.

A special thank you to Ben Nikaido, whose generosity in allowing me to work under him has been a crucial part of my research journey. His willingness to share knowledge, offer guidance, and assist with both my project and his own has been truly invaluable.

Additionally, I extend my appreciation to my colleagues and peers at both NPS and SJSU, whose discussions, collaboration, and encouragement have helped shape this project.

Thank you all for your contributions to this project.

Contents

Nomenclature **1**

1 Introduction **3**

1.1 Motivation 3

1.2 Literature Review 5

1.3 Project Proposal 11

1.4 Methodology 13

1.4.1 Phase I: CFD-Guided Flowfield Investigation 13

1.4.2 Phase II: Hardware Development and Fabrication . . . 14

1.4.3 Phase III: Experimental Validation Strategy 14

1.4.4 Integration of Simulation and Experiment 15

2 Manufacturing and Fabrication **16**

2.1 Overview of Manufacturing Requirements 16

2.2 Consumer-Grade Prototyping: Bambu Lab Printers 17

2.3 Industrial Prototyping: Stratasys F370 and F900 Systems . . 18

2.3.1 Stratasys F370: Mid-Tier Industrial 3D Printing 18
2.3.2 Stratasys F900: High-End Industrial ULTEM Manufacturing 20
2.3.3 Vacuum Oven for Filament Preparation 21
2.3.4 M2 Cusing Metal Additive Manufacturing 23

3 Computational Fluid Dynamics (CFD) Simulations 26

3.1 2D Geometry and Domain Setup 27
3.2 2D Meshing Strategy 27
3.3 2D Physics Models and Solver Configuration 28
3.4 2D Exploratory Simulation Results 29
3.5 3D CFD Development 30
3.6 CFD Results 30
3.6.1 Pre-Startup With Incorrect Boundary Conditions . . . 31
3.6.2 First Successful Start 31
3.6.3 End Goal of a Standing Shockwave 32
3.7 CFD Validation Strategy 33

4 Experimental Setup 34

4.1 Experimental Setup 34
4.1.1 Prototype Iterations 34
4.2 Alternative Injection Geometry: Metal Pipe Assemblies 42
4.3 Manifold Setup 44
4.4 Schlieren Camera Setup 46

4.5 Initial Schlieren Imaging Results 48

5 Results **50**

5.1 CFD and Experimental Results for Metal Pipe Injection Geometry 50

5.1.1 Experimental Schlieren Imaging Results 52

6 Discussion **54**

7 Application of Aerospace Engineering Science and Design Constraints **57**

7.1 Application of Aerospace Engineering 58

7.1.1 Aerodynamics and High Speed Flow Physics 58

7.1.2 Propulsion and Inlet Dynamics 58

7.1.3 Flight Mechanics and Flow Stability 59

7.1.4 Aerospace Structures and Materials 59

7.1.5 Manufacturability and Additive Manufacturing Science 59

7.2 Incorporation of Engineering Design Constraints 60

7.2.1 Economic Considerations 60

7.2.2 Environmental and Sustainability Constraints 61

7.2.3 Social and Political Constraints 61

7.2.4 Ethical and Professional Responsibilities 61

7.2.5 Health and Safety Constraints 62

7.2.6 Manufacturability Constraints 62

7.2.7 Sustainability Considerations 63
7.3 Summary 63

8 Conclusions and Future Work **65**

List of Tables

4.1 Tri-nozzle injection hole diameters and corresponding flow areas. 36

List of Figures

1.1 Shock wave structures in an inlet at Mach 2, illustrating compression and boundary layer interactions. 5
1.2 Schlieren imaging of inlet flow before and during un-start. . . 6
1.3 NASA X-43A Hyper-X air vehicle. 7
1.4 The X-51A Waverider hypersonic test vehicle. 7
1.5 Mach number distribution in a complex inlet, highlighting flow separation and shock movement under un-start conditions. . . 8

2.1 Bambu Lab consumer-grade printer used for rapid prototyping, orientation testing, and fit verification. 18
2.2 Stratasys F370 industrial printer used for high-strength polycarbonate fabrication and soluble-support prototyping. 20
2.3 Stratasys F900 industrial printer used exclusively for printing high-temperature ULTEM components for final hardware fabrication. 22

2.4 Vacuum oven used to dry hygroscopic filaments such as polycarbonate and ULTEM before printing in the F370 and F900. 23
2.5 M2 Cusing metal additive manufacturing system used for producing high-strength, laser-sintered metal components. 25

3.1 2D geometry of the Mach 4 wind tunnel simulation domain used in CFD. 27
3.2 Mesh structure across the full domain, showing refinement in critical areas. 28
3.3 Zoomed-in view of prism layers and near-wall refinement in the test section. 28
3.4 2D simulation of un-start caused by fixed-injection louvre geometry. 29
3.5 Unsuccessful startup case showing shock diamonds caused by incorrect outlet pressure. 31
3.6 Half-depth 3D simulation showing the tri-nozzle configuration. 32

4.1 PLA fit-check insert used to verify geometry, mounting alignment, and clearances inside the Mach 4 test section. 35
4.2 Polycarbonate tri-nozzle front section after failure. The failure is consistent with vibration-induced breakup. 37
4.3 Fragments of the Polycarbonate tri-nozzle recovered from inside the tunnel. 38
4.4 Intact ULTEM tri-nozzle prior to testing. 39

4.5 Rear section of the ULTEM nozzle showing open-back design for support removal. 39
4.6 Front-end structural failure of the ULTEM nozzle after Mach 4 startup forces. 40
4.7 Close-up of ULTEM nozzle prong failure, indicating vibration-driven cyclic loading. 40
4.8 Top-view failure of the ULTEM nozzle showing breakup of the upper channel region. 41
4.9 0.66 inch pipe with a custom valve fitting 42
4.10 0.54 inch pipe with 1/8inch holes for mass injection with custom PLA mounting 43
4.11 CAD model of the 3D-printed PC manifold used for secondary injection. 44
4.12 Experimental manifold setup with reinforced tubing. 45
4.13 Nitrogen-tank injection setup capable of supplying 120–200 psi through the manifold. 45
4.14 The actual schlieren camera used in the experiment 46
4.15 Schlieren system integrated into the Mach 4 wind tunnel. . . . 47
4.16 Sample Schlieren frame extracted during mass injection using the metal nozzle insert. 48
4.17 Bladed metal nozzle used for mass injection during early testing. 49

5.1 Ansys Fluent simulation of the tunnel with a 0.6 in diameter hole at the second throat. 51
5.2 Ansys Fluent simulation of the tunnel with a 0.4 in diameter hole at the second throat. 52
5.3 Live Schlieren image captured during tunnel operation with a 0.66 in diameter pipe installed and no secondary mass injection. 52

Nomenclature

A	Flow area
d	Orifice or hole diameter
$\dot{m}$	Mass flow rate
M	Mach number
p	Static pressure
p_0	Total (stagnation) pressure
T	Static temperature
T_0	Total (stagnation) temperature
ρ	Density
Re	Reynolds number
y^+	Dimensionless wall distance
γ	Ratio of specific heats
μ	Dynamic viscosity

CFD	Computational Fluid Dynamics
RANS	Reynolds Averaged Navier Stokes
SST	Shear Stress Transport
SWBLI	Shock Wave Boundary Layer Interaction
NPS	Naval Postgraduate School
PLA	Polylactic Acid
PC	Polycarbonate
PEI	Polyetherimide (ULTEM)

Chapter 1

Introduction

1.1 Motivation

Hypersonic flight presents some of the most demanding challenges in aerospace engineering, arising from strong shock wave interactions, extreme thermal loads, and inherently unsteady flow dynamics. At Mach 4, one of the most critical instabilities is *un-start*—a sudden disruption of supersonic inlet flow that can lead to complete loss of stability in both wind tunnels and hypersonic vehicles. This phenomenon is particularly detrimental for scramjet propulsion systems, where maintaining a stable supersonic combustor flow is essential for sustained operation.

Understanding and mitigating *un-start* is therefore a key requirement for hypersonic vehicle development, propulsion efficiency, and experimental

wind tunnel reliability. Computational Fluid Dynamics (CFD) provides insight into the flow conditions and mechanisms that trigger un-start; however, experimental validation remains indispensable to ensure predictive accuracy and applicability to real-world systems.

This project addresses that need by combining high-fidelity CFD simulations with controlled experiments in the Naval Postgraduate School's Mach 4 hypersonic wind tunnel—a rare facility capable of sustaining repeatable Mach 4 flow in a laboratory environment. The study will (i) identify critical flow conditions leading to un-start, (ii) design and test injection-based mechanisms to deliberately induce un-start, and (iii) compare numerical predictions against experimental Schlieren imaging and pressure measurements. By integrating these approaches, the research aims to improve predictive models, refine un-start mitigation strategies, and enhance the reliability of hypersonic wind tunnel testing for future aerospace applications.

1.2 Literature Review

Fundamentals of Un-Start

A supersonic or hypersonic *un-start* is a flow instability that occurs in air-breathing propulsion systems at high flight speeds. It is characterized by the breakdown of supersonic inlet flow, driven by shock wave displacement, boundary-layer separation, and even flow reversal [1, 2, 3]. If the boundary layer grows excessively inside the inlet, or if combustion-induced backpressure rises too high, the incoming air may reverse direction and spill from the inlet, resulting in a catastrophic loss of stability.

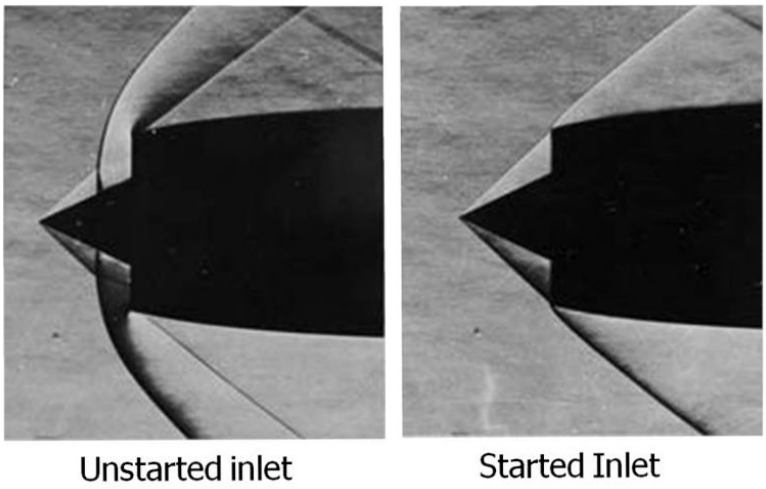


Figure 1.1: Shock wave structures in an inlet at Mach 2, illustrating compression and boundary layer interactions.

The root cause of *un-start* lies in the interaction between shock waves and the boundary layer (SWBLI). Under adverse conditions—such as increas-

ing backpressure, large pressure gradients, or changes in angle of attack—the shock system moves upstream, causing inlet choking and a sudden collapse of supersonic flow.

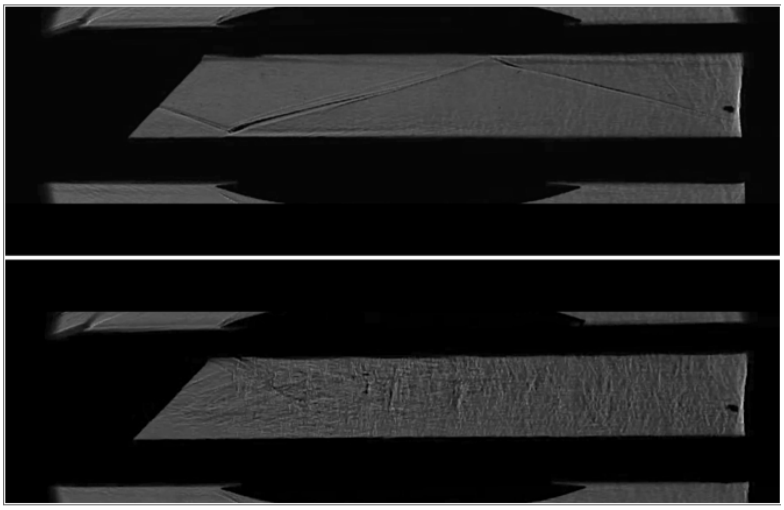


Figure 1.2: Schlieren imaging of inlet flow before and during un-start.

Experimental Evidence and Hypersonic Flight Programs

NASA's X-43A scramjet program and the U.S. Air Force's X-51A Waverider both provide high-profile examples of flight failures due to *un-start*. In 2001, an X-43A test ended in destruction after an inlet instability triggered un-start [4]. The X-51A successfully sustained Mach 5.1 flight for 210 seconds in its fourth test, but its second flight ended prematurely when an inlet un-start disrupted combustion, forcing a controlled crash [5, 6].



Figure 1.3: NASA X-43A Hyper-X air vehicle.

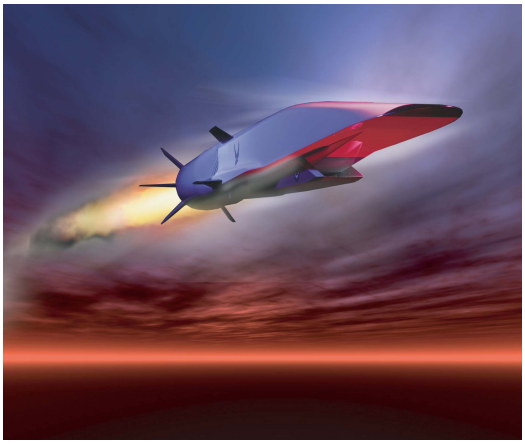


Figure 1.4: The X-51A Waverider hypersonic test vehicle.

Mass Injection as a Trigger

Beyond flight data, controlled un-start has been induced experimentally. Do et al. [7] demonstrated that transverse mass injection into a Mach inlet disrupted the supersonic core, displaced the shock system, and caused boundary-layer separation, ultimately producing an un-start. Their results highlighted how injection-driven disturbances strongly couple with inlet stability, providing valuable validation data for CFD studies.

Role of CFD in Understanding Un-Start

Since large-scale flight experiments are prohibitively expensive, Computational Fluid Dynamics (CFD) has become indispensable for investigating un-start phenomena. CFD enables researchers to study SWBLI, flow separation, and pressure fluctuations at a fraction of the cost of physical testing [8, 9].

For example, a NASA Glenn study simulated an inward-turning supersonic inlet at Mach 1.7 using Wind-US, capturing upstream shock movement before the predicted backpressure limit [8]. Other studies have applied Kantrowitz theory to supersonic inlet cascades and confirmed that CFD predictions closely matched experiments [9]. Yu et al. [10] combined CFD and continuously variable wind tunnel tests, showing excellent agreement in pressure distributions.

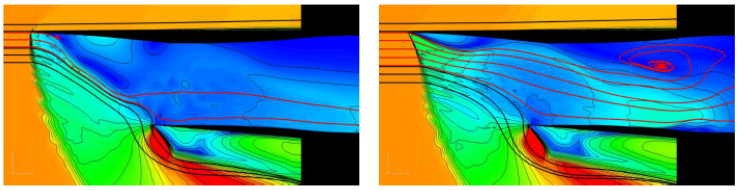


Figure 1.5: Mach number distribution in a complex inlet, highlighting flow separation and shock movement under un-start conditions.

Direct Relevance to the NPS Mach 4 Tunnel

One of the most important studies for this project was conducted by Nikaido and Hobson [11], who used Reynolds-Averaged Navier–Stokes (RANS) CFD

solvers (OVERFLOW and CREATE-AV Kestrel) to investigate Mach 4 inlet-isolator un-start. Their simulations, validated in the Naval Postgraduate School's Mach 4 wind tunnel, showed un-start induced by a fan-like louver system. The present study builds directly on this work, extending it by testing injection-based mechanisms for un-start rather than mechanical louvers.

More recently, Plum et al. [12] characterized the same Mach 4 tunnel, showing Mach numbers ranging from 3.91 to 4.41 with secondary sidewall flows. These results provide the baseline flow uniformity and turbulence data required for accurate experimental design.

Recent Advancements in Un-Start Research

Recent high-fidelity simulations have expanded understanding of un-start. Redding et al. (2024) used the Eilmer solver to show that both angle of attack and pitch rate strongly affect un-start onset, highlighting the need for dynamic control strategies in hypersonic inlets [13]. Zahrolayali et al. (2022) explored localized heat sources to mitigate SWBLI under throttling conditions, finding that thermal management improved pressure recovery and reduced distortion [14]. Li et al. (2023) investigated plug-throttling versus thermal-choking un-start in twin-duct inlets, showing thermal choking created a larger restart hysteresis loop, making recovery more difficult [15].

Summary

The study of *un-start* in supersonic and hypersonic inlets has advanced through decades of CFD modeling, wind tunnel testing, and limited flight data. While CFD has proven effective at predicting un-start onset and propagation, experimental validation remains essential, especially under Mach 4 conditions. This project contributes to that effort by integrating CFD with targeted experiments in the NPS Mach 4 tunnel, extending prior louver-based studies to injection-driven un-start mechanisms. The resulting insights will improve predictive models, guide inlet design, and advance high-speed propulsion system reliability.

1.3 Project Proposal

The objective of this project was to investigate the dynamics of Mach 4 *un-start* phenomena using both computational and experimental approaches. The computational phase employed Computational Fluid Dynamics (CFD) to simulate Mach 4 inlet flow and identify the critical conditions that trigger *un-start*. Key parameters—including pressure distribution, shock wave formation, and transient flow behavior—were analyzed to establish thresholds for *un-start* initiation.

In parallel, an experimental campaign was conducted in the Naval Postgraduate School's Mach 4 hypersonic wind tunnel. Injection-driven *un-start* was deliberately attempted using an injection-based louvre system, rather than relying on the tunnel's existing area-reduction mechanism. Flow disturbances were introduced through controlled secondary injection, with real-time measurements acquired from wall-mounted pressure transducers and Schlieren imaging systems. This configuration ensured that the observed phenomena represented full-system inlet behavior and allowed direct comparison with CFD predictions.

By integrating high-fidelity CFD simulations with controlled wind tunnel testing, this study extended previous louvre-based *un-start* research and developed a CFD-guided framework for injection-driven *un-start* investigations. The results provided actionable insights into predictive modeling accuracy, injector design limitations, and experimental constraints relevant

to hypersonic inlet research and future experimental methodologies.

1.4 Methodology

This project uses a three-phase methodology to investigate Mach 4 un-start: (i) computational analysis using CFD to understand flow behavior and guide hardware design, (ii) fabrication of injector hardware through iterative additive manufacturing, and (iii) experimental validation in the Naval Postgraduate School (NPS) Mach 4 wind tunnel. This chapter provides a high-level overview of the research process, while detailed CFD and experimental procedures are presented in later chapters.

1.4.1 Phase I: CFD-Guided Flowfield Investigation

Computational Fluid Dynamics (CFD) served as the foundation for understanding the baseline Mach 4 flow, predicting un-start onset, and evaluating the effectiveness of secondary mass injection. Initial 2D simulations examined shock formation, boundary-layer behavior, and the interaction of injected flow with the supersonic core. These insights guided the selection of injection geometries and informed the development of 3D models.

The objective of this phase was not only to replicate Mach 4 startup, but also to explore injection-based mechanisms capable of disturbing the inlet sufficiently to trigger un-start. The final CFD output consisted of nozzle placement recommendations, predicted shock structures, expected mass-flow requirements, and survivability constraints for the injection hardware.

1.4.2 Phase II: Hardware Development and Fabrication

The CFD results were translated into physical hardware through an iterative manufacturing process. Early concepts were prototyped using consumer-grade printers to verify geometry and fit within the tunnel window. Subsequent versions were produced using polycarbonate and ULTEM on industrial Stratasys platforms, followed by metal additive manufacturing for components requiring higher structural strength.

Each prototype was evaluated under wind-tunnel startup conditions, and failure modes (vibration, thermal softening, or mechanical fracture) were used to refine geometry, material selection, and manufacturing tolerances. This iterative approach ensured that the final design met the structural, flow distribution, and integration requirements for Mach 4 testing.

1.4.3 Phase III: Experimental Validation Strategy

The final phase involves validating CFD predictions in the NPS Mach 4 wind tunnel. A controlled mass-injection manifold delivers high-pressure air or nitrogen through the fabricated nozzles to intentionally disturb the test-section flow. Schlieren imaging provides visualization of shock motion and density gradients, while wall-mounted pressure transducers measure unsteady pressure behavior during the onset of un-start.

The experimental plan allows direct comparison between predicted and observed shock structures, flow separation behavior, and overall un-start dynamics. Discrepancies between simulation and experiment will be used to refine turbulence modeling, mass-flow estimates, and nozzle geometry for future tests.

1.4.4 Integration of Simulation and Experiment

The methodology follows a simulation–fabrication–validation loop. CFD informs hardware design; experimental data validate CFD assumptions; and hardware survivability feeds back into both design and simulation constraints. This integrated approach systematically reduces uncertainty in predicting and inducing Mach 4 un-start and establishes a repeatable framework for future hypersonic inlet studies.

Chapter 2

Manufacturing and Fabrication

2.1 Overview of Manufacturing Requirements

The manufacturing requirements were dictated primarily by three constraints:

1. **Survivability in Mach 4 flow.** The wind tunnel imposes extremely high aerodynamic loading, reaching forces exceeding 16 kN on the wind blade structure.

2. **Ability to inject controlled secondary mass flow.** The design must survive high-pressure nitrogen injection of 50–120 PSI while delivering a target mass flow rate of 0.05–0.07 kg/s.

3. **Interface compatibility.** All components, including manifolds and mounting hardware, must fit within the existing NPS tunnel window

ports and seal against the sidewalls.

These constraints directly influenced material choices, nozzle geometry, and overall manufacturing approaches.

2.2 Consumer-Grade Prototyping: Bambu Lab Printers

One of the primary tools used during the early manufacturing phase was the Bambu Lab series of high-end consumer 3D printers. These machines were ideal for rapid prototyping because they offer fast print speeds, high dimensional accuracy, and reliable multi-material capabilities. Their primary purpose in this project was to prototype components, evaluate print orientation, and verify geometric fit before committing to more expensive manufacturing methods.

Print orientation is a critical consideration in additive manufacturing. The direction of the printed layers determines where support structures are placed and directly affects the overall structural strength of the part. Because 3D printed components are inherently weaker along their layer lines, testing multiple orientations helps identify the configuration that provides the highest strength for load-bearing features. The Bambu printers allowed these orientation experiments to be performed quickly and cost-effectively.

These printers also enabled rapid fit checks inside the Mach 4 tunnel

window ports and against other printed assemblies. By validating geometry and layout using inexpensive prototype materials, later iterations—such as polycarbonate, ULTEM, or metal 3D prints—were manufactured with higher confidence and reduced risk of costly failures.



Figure 2.1: Bambu Lab consumer-grade printer used for rapid prototyping, orientation testing, and fit verification.

2.3 Industrial Prototyping: Stratasys F370 and F900 Systems

2.3.1 Stratasys F370: Mid-Tier Industrial 3D Printing

The Stratasys F370 is a mid-tier industrial-grade FDM printer used for manufacturing stronger and more durable thermoplastic components. For this

project, the machine was configured exclusively for polycarbonate (PC) printing. Polycarbonate offers significantly higher toughness and heat resistance than PLA, but it also introduces stricter manufacturing requirements.

PC requires a nozzle temperature between 260C and 310C, as well as an actively heated chamber held at approximately 90C. This prevented rapid cooling that would otherwise cause part warping, cracking, or delamination. Unlike consumer printers, the F370 maintains these thermal conditions with high stability, enabling reliable production of complex PC parts.

A major advantage of the F370 is its use of soluble support materials. This capability is critical for parts with internal cavities or intricate geometries. Post-processing by dissolving the support material avoids the risk of mechanically breaking delicate overhangs or thin features. This is especially important for materials like ULTEM, whose support material is notoriously difficult to remove manually.

The F370 served as an intermediate fabrication platform: more capable than consumer printers but less costly to operate than high-temperature ULTEM-capable machines like the F900.



Figure 2.2: Stratasys F370 industrial printer used for high-strength polycarbonate fabrication and soluble-support prototyping.

2.3.2 Stratasys F900: High-End Industrial ULTEM Manufacturing

The Stratasys F900 is a top-tier industrial 3D printer with a large build volume of approximately 3 ft $\times$ 2 ft $\times$ 3 ft, designed to manufacture aerospace-grade polymer components. For this research, the F900 was configured ex-

clusively to print ULTEM (PEI), a high-performance thermoplastic widely used in military aviation and space systems due to its exceptional strength, thermal resistance, and environmental durability.

ULTEM printing requires extreme thermal conditions: a nozzle temperature of approximately 370C and a chamber temperature near 180C. These requirements ensure proper layer adhesion and prevent thermal-induced warping. The F900's precision temperature control makes it one of the few printers capable of consistently producing high-quality ULTEM hardware.

ULTEM will be used for the final version of the wind-blade injection system after all geometry, tolerances, and fit checks have been validated using the Bambu Lab printers and intermediate PC prototypes. Because ULTEM printing is significantly more expensive—both in material cost and machine runtime—the F900 is reserved for final, validated designs only.

2.3.3 Vacuum Oven for Filament Preparation

Both the Stratasys F370 and the Stratasys F900 rely on high-performance filaments—polycarbonate (PC) and ULTEM (PEI), respectively—that are extremely sensitive to moisture absorption. These materials are hygroscopic, meaning they readily absorb moisture from the surrounding air. Even small amounts of absorbed water can lead to severe print defects, including:

- Bubbling and surface pitting,



Figure 2.3: Stratasys F900 industrial printer used exclusively for printing high-temperature ULTEM components for final hardware fabrication.

- Internal voids and porosity,
- Weakened interlayer bonds,
- Dimensional inaccuracy due to steam expansion,
- Poor surface finish and delamination.

To prevent these issues, all PC and ULTEM filament spools must be baked in a vacuum oven prior to printing. The vacuum environment lowers the boiling point of the absorbed moisture, allowing it to be removed efficiently without damaging the filament. This drying process is essential for maintaining the mechanical integrity and print quality required for both prototyping and final hardware fabrication.

The vacuum oven was used routinely throughout the project to dry filament before loading it into the F370 or F900. Without this step, high-temperature printing of PC or ULTEM would reliably fail or produce structurally unsound components, making the vacuum oven a critical part of the manufacturing workflow.



Figure 2.4: Vacuum oven used to dry hygroscopic filaments such as polycarbonate and ULTEM before printing in the F370 and F900.

2.3.4 M2 Cusing Metal Additive Manufacturing

The M2 Cusing system is a high-end metal additive manufacturing machine designed for producing dense, high-strength components with intricate internal geometry. Unlike polymer-based printers, the M2 uses metal powder as its raw material and builds parts layer by layer using a precision laser-melting process. Each layer—typically on the order of tens of microns—is

spread across the build plate before being selectively fused by a high-power laser to form the final part geometry.

During operation, the build chamber is overpressurized with an inert gas, typically argon, to prevent oxidation and unwanted chemical reactions. Maintaining an oxygen-free environment is critical for ensuring metallurgical quality, preventing micro-cracking, and producing structurally sound aerospace-grade hardware.

Because the process relies on extremely fine metal powder, strict safety procedures are required. The powder is a significant inhalation hazard, and appropriate personal protective equipment (PPE) must be worn at all times. This includes respirators, gloves, antistatic clothing, and protective eyewear. Handling, loading, and recovering metal powder from the machine must be done with specialized vacuum systems designed specifically for combustible dust.

Post-processing of metal prints is substantially more labor-intensive than polymer-based additive manufacturing. All support structures are made from solid metal and therefore must be removed using industrial tools such as bandsaws, grinders, chisels, or CNC machining operations. Care must be taken during support removal to avoid damaging the primary features of the part, especially for thin-walled components or internal channels.

Despite the complexity and cost, the M2 Cusing system produces the strongest and most durable components available in this project and

represents the ultimate manufacturing route for hardware that must survive the aerodynamic loading inside the Mach 4 wind tunnel.



Figure 2.5: M2 Cusing metal additive manufacturing system used for producing high-strength, laser-sintered metal components.

Chapter 3

Computational Fluid Dynamics (CFD) Simulations

This chapter presents the full numerical investigation used to understand Mach 4 startup, shock behavior, and un-start initiation in the Naval Postgraduate School (NPS) Mach 4 wind tunnel. The following sections summarize the simulation geometry, mesh generation, physics models, and iterative CFD development that informed the injector design used in experimental testing.

3.1 2D Geometry and Domain Setup

To replicate the Mach 4 wind tunnel flowfield, a simplified two-dimensional geometry was created based on 3D laser scans of the test section. A 1.06 m segment containing both the throat and the test section was modeled to balance computational cost and geometric fidelity.

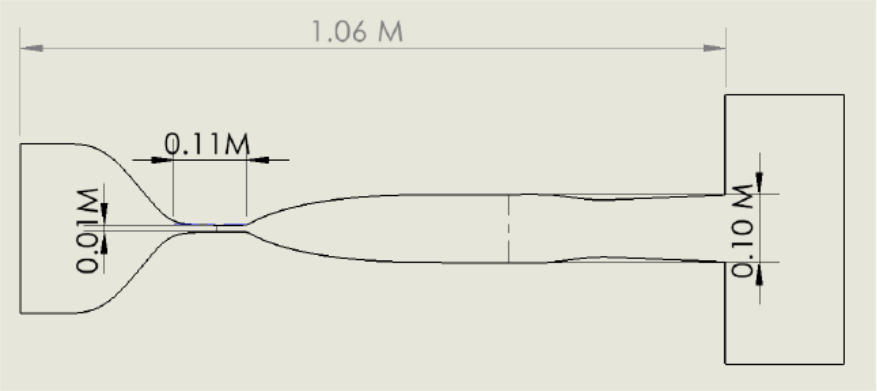


Figure 3.1: 2D geometry of the Mach 4 wind tunnel simulation domain used in CFD.

3.2 2D Meshing Strategy

The 2D domain was meshed using polygonal cells with refinement concentrated near the throat and the test section where strong shock gradients are expected. Prism layers were added along walls to capture boundary-layer development and resolve viscous effects.

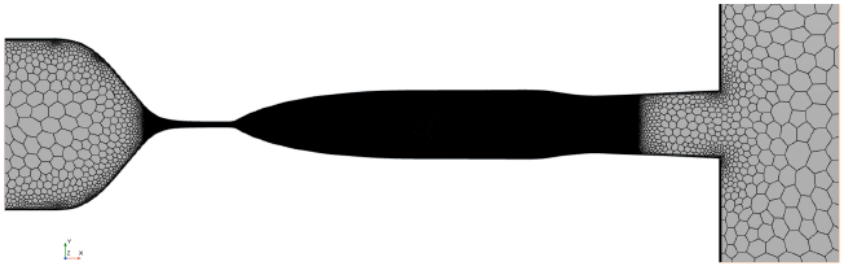


Figure 3.2: Mesh structure across the full domain, showing refinement in critical areas.

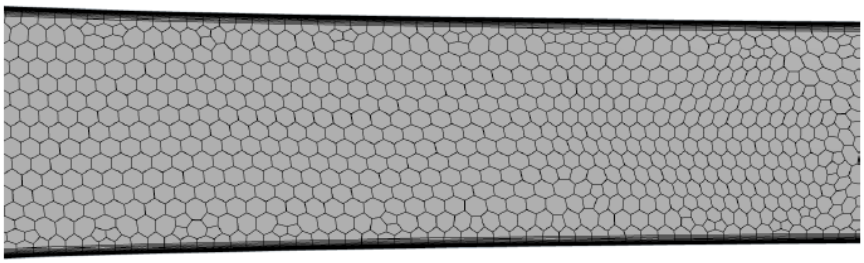


Figure 3.3: Zoomed-in view of prism layers and near-wall refinement in the test section.

3.3 2D Physics Models and Solver Configuration

Two flow regimes were simulated:

- **Inviscid baseline:** used to evaluate tunnel startup and core shock formation.

- **SST k–ω turbulence model:** used to resolve boundary layers and shock–boundary-layer interaction.

Boundary conditions included $P_t = 10$ atm, $T_t = 300$ K at the inlet, an outlet reference pressure of $P = 0$ Pa, adiabatic no-slip walls, and symmetry along the tunnel centerline.

3.4 2D Exploratory Simulation Results

Two approaches for inducing un-start were investigated in 2D:

- **Rotating louvres:** generated over 16,200 N of drag but failed to trigger a global un-start.
- **Fixed-channel mass injection:** produced shock formation, strong flow reversal, and successful un-start, making it the preferred approach for 3D refinement.

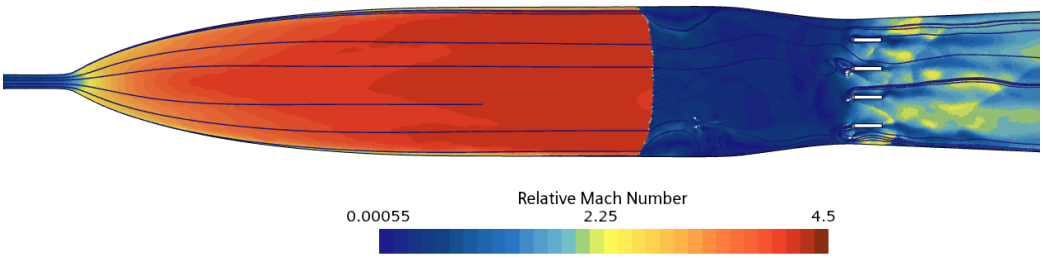


Figure 3.4: 2D simulation of un-start caused by fixed-injection louvre geometry.

3.5 3D CFD Development

With injection-induced un-start demonstrated in 2D, 3D simulations were performed to evaluate practical injector configurations. A half-depth model with a symmetry plane was used to reduce computational cost while preserving three-dimensional flow structures.

Three nozzle configurations were evaluated:

- **Long nozzles:** extended into the Schlieren window; produced bow shocks.
- **1 inch offset nozzles:** produced full un-start but still generated bow shocks.
- **Tri-nozzle configuration:** generated a near-normal shock centered in the Schlieren window; selected for physical testing.

Mesh refinement at the throat (0.2 mm) and test section (0.8 mm) resulted in approximately one million cells.

3.6 CFD Results

The CFD results evolved through several iterations that refined boundary conditions and validated the numerical setup.

3.6.1 Pre-Startup With Incorrect Boundary Conditions

Initial 3D simulations produced shock diamonds but failed to start the tunnel. The cause was traced to an incorrect outlet pressure ratio.

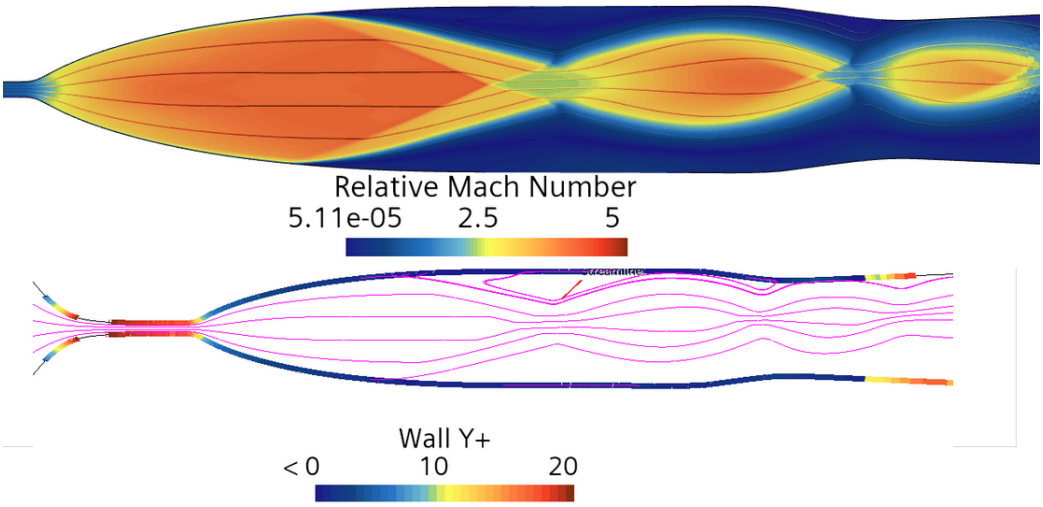


Figure 3.5: Unsuccessful startup case showing shock diamonds caused by incorrect outlet pressure.

3.6.2 First Successful Start

With the outlet corrected to 1000 Pa, the tunnel achieved full Mach 4 startup and subsequently exhibited a complete start event. Now we are able to create designs that can reliably unstart the wind tunnel

3.6.3 End Goal of a Standing Shockwave

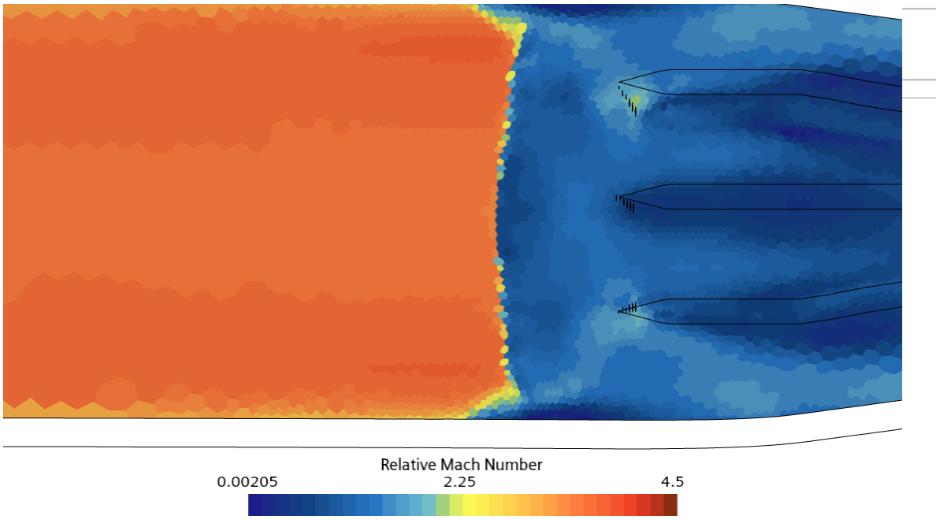


Figure 3.6: Half-depth 3D simulation showing the tri-nozzle configuration.

The configuration shown in Figure 3.6 represents the ultimate objective of this project: to reliably generate a stationary, repeatable standing shockwave inside the Mach 4 test section. Establishing a controlled, steady shock structure is essential for future experimental studies involving shock–boundary-layer interaction, un-start onset, flow control concepts, and model validation.

The tri-nozzle design was developed specifically to achieve this goal. It injects mass into the supersonic core flow through three primary injection locations: one centered on the mid-plane and two additional ports located 1.3 inches off-center. This arrangement ensures that the injected flow produces a symmetric disturbance capable of displacing and reshaping the natural Mach 4 shock train. By distributing mass addition across multiple

lateral positions rather than a single jet, the tri-nozzle promotes a more uniform blockage effect, which is necessary for forming a nearly normal, stable shockwave in the Schlieren window.

CFD results indicate that this configuration is capable of creating a well-defined standing shock under the correct inlet conditions and injection flow rates. These results represent numerical predictions only; experimental testing did not achieve a sustained standing shock due to structural survivability limits and operational constraints discussed in later sections. Achieving this behavior experimentally would provide a controlled platform for studying un-start physics, validating numerical models, and performing high-resolution Schlieren imaging of shock dynamics. Ultimately, the tri-nozzle serves as both a diagnostic tool and a flow-control mechanism, enabling the isolation and examination of Mach 4 shock behavior in a way that has not been previously implemented in the NPS wind tunnel.

3.7 CFD Validation Strategy

CFD predictions will be validated using wall-mounted pressure transducers and Schlieren imaging during wind tunnel testing. Experimental shock positions and un-start onset will be compared to simulation results to refine model accuracy.

Chapter 4

Experimental Setup

4.1 Experimental Setup

4.1.1 Prototype Iterations

Following the failure of the airblade injector system to unstart the tunnel, a new approach was required. CFD simulations of the tri-nozzle concept showed that a protruding nozzle extending from the mounting bracket to the test-section windows would generate stronger shocks and allow direct visualization of nozzle-induced disturbances. This resulted in a series of prototype iterations fabricated from PLA, Polycarbonate (PC), and ULTEM.

PLA Fit Check

The first prototype was printed in PLA using a Bambu Lab system. This part was not intended for high-speed testing; instead, it served as a fit-check model to ensure that the tri-nozzle geometry could be inserted into the tunnel, wedge securely into the second throat, and remain held in place by Mach 4 aerodynamic drag forces.

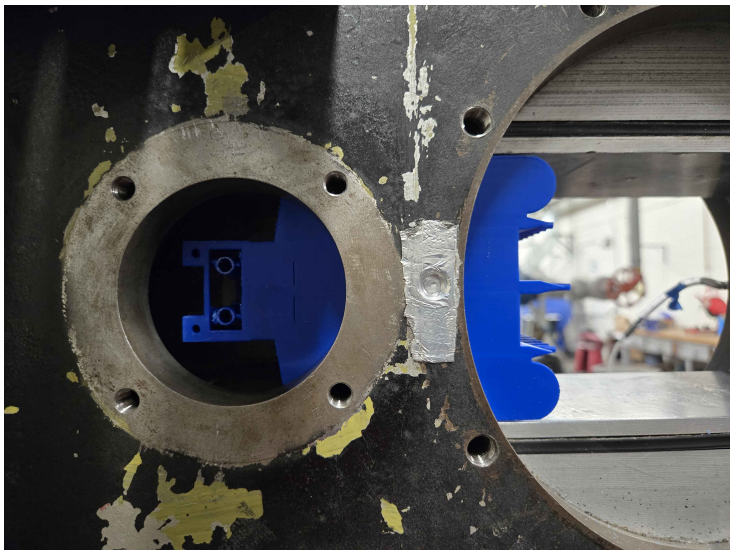


Figure 4.1: PLA fit-check insert used to verify geometry, mounting alignment, and clearances inside the Mach 4 test section.

Tri-Nozzle Injection Hole Sizing

The tri-nozzle incorporates twelve injection holes arranged symmetrically along the nozzle face. Indices 1–12 correspond to the circumferential order of the holes beginning at the top and proceeding clockwise. The hole sizes increase toward the mid-plane to increase mass-flow delivery where blockage

effects are strongest. Table 4.1 lists each hole diameter and flow area.

$$\begin{aligned} A_{\text{total}} &= \sum_{i=1}^{12} A_i \\ &= 30.066 \text{ mm}^2 \end{aligned} \tag{4.1}$$

Thus, the array provides the same total flow area as a single 6.18 mm (0.243 in) jet, but distributed to improve mixing, reduce local loading, and enhance blockage uniformity.

Table 4.1: Tri-nozzle injection hole diameters and corresponding flow areas.

Index	A_i (mm^2)	d_i (mm)	d_i (in)
1	0.8107	1.016	0.040
2	1.8241	1.524	0.060
3	2.4829	1.778	0.070
4	3.2429	2.032	0.080
5	4.1043	2.286	0.090
6	5.0671	2.540	0.100
7	5.0671	2.540	0.100
8	4.1043	2.286	0.090
9	3.2429	2.032	0.080
10	2.4829	1.778	0.070
11	1.8241	1.524	0.060
12	0.8107	1.016	0.040

Polycarbonate Prototype

The first operational tri-nozzle was printed in Polycarbonate (PC). PC was selected because:

- Its material data sheet indicated sufficient strength for expected tunnel loads, and
- PC uses soluble support material, which was essential due to internal nozzle cavities.

During the first run, the tunnel did not reach full Mach 4. The PC nozzle survived approximately 10 seconds before developing large-amplitude vibrations and failing catastrophically.



Figure 4.2: Polycarbonate tri-nozzle front section after failure. The failure is consistent with vibration-induced breakup.



Figure 4.3: Fragments of the Polycarbonate tri-nozzle recovered from inside the tunnel.

ULTEM Prototype

The next iteration was printed in ULTEM, the strongest thermoplastic available. To increase survivability, the nozzle was coated in epoxy. Because ULTEM supports are not soluble, the rear of the nozzle was redesigned with an open-back geometry so tools could be used to remove internal supports manually. A machined metal plate was later epoxied into place to restore structural continuity.

During the Mach 4 run, the ULTEM nozzle survived long enough for Schlieren imaging but ultimately failed due to severe vibration. The test also showed that even without injection, the nozzle caused startup difficulty—consistent with CFD-predicted blockage.

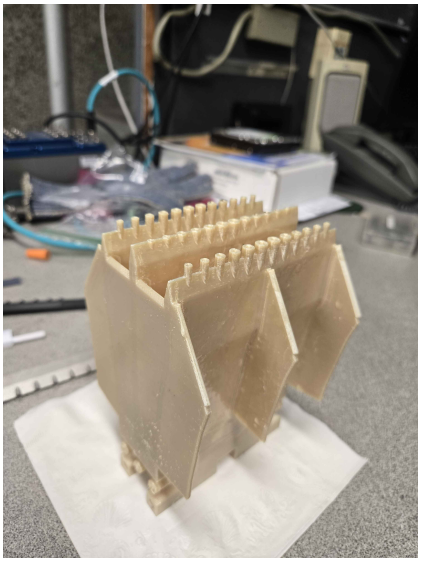


Figure 4.4: Intact ULTEM tri-nozzle prior to testing.

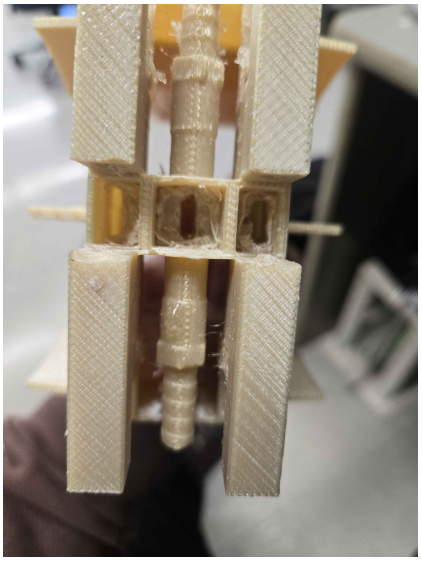


Figure 4.5: Rear section of the ULTEM nozzle showing open-back design for support removal.

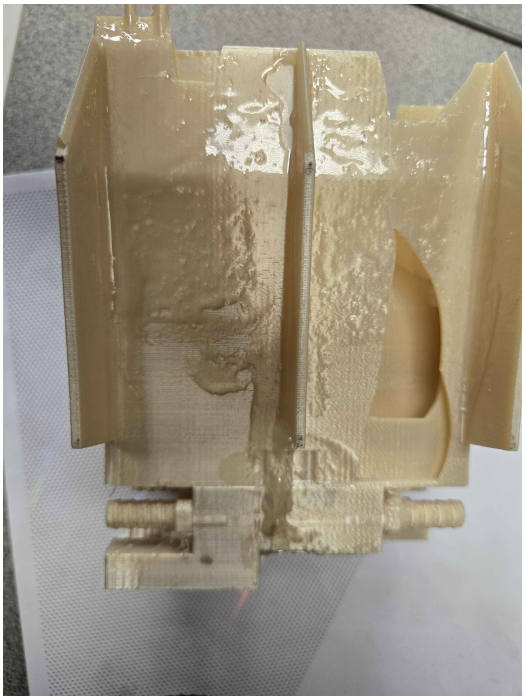


Figure 4.6: Front-end structural failure of the ULTEM nozzle after Mach 4 startup forces.

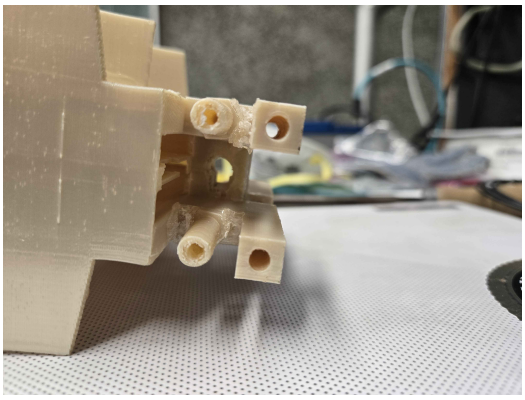


Figure 4.7: Close-up of ULTEM nozzle prong failure, indicating vibration-driven cyclic loading.

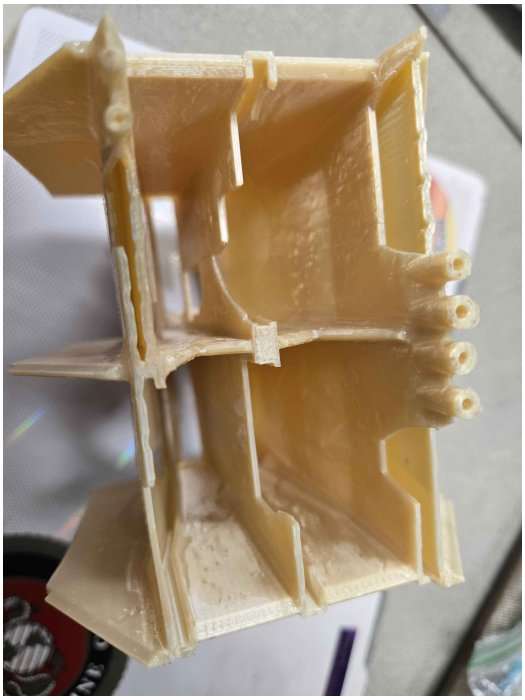


Figure 4.8: Top-view failure of the ULTEM nozzle showing breakup of the upper channel region.

The tri-nozzle concept was ultimately abandoned after testing confirmed that the internal support structure at the rear of the nozzle created a significant geometric blockage within the test section. This blockage prevented the tunnel from fully starting, producing only a semi-started flow condition even before mass injection was introduced. Although a metal additively manufactured version of the nozzle had been proposed to eliminate the internal support material and restore the intended flow path, fabrication was halted due to the federal government shutdown, which temporarily suspended all purchasing and manufacturing operations. Even if metal pro-

duction had been possible, the cumulative evidence from the polycarbonate and ULTEM failures indicated that the overall nozzle architecture may not be structurally viable for Mach 4 loading without a complete redesign. Consequently, continuing to pursue the tri-nozzle configuration was determined to be neither practical nor an efficient use of remaining resources.

4.2 Alternative Injection Geometry: Metal Pipe Assemblies



Figure 4.9: 0.66 inch pipe with a custom valve fitting

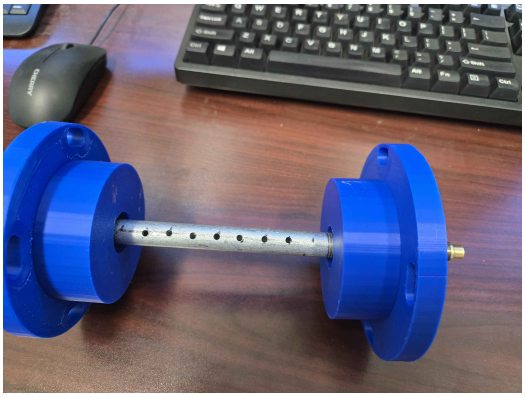


Figure 4.10: 0.54 inch pipe with 1/8inch holes for mass injection with custom PLA mounting

After the tri-nozzle design was abandoned, a simpler and more cost-effective injection concept was pursued. Metal pipes of varying diameters were selected to evaluate whether a minimal-geometry injector could generate sufficient disturbance to initiate unstart. Two pipes were tested: one with a diameter of 0.66 in and another with a diameter of 0.54 in, the latter drilled with 1/8-in injection holes along its length. Both pipes were supported using custom PLA mounts that secured the assemblies within the test-section window. One end of each pipe was left open to interface directly with the high-pressure nitrogen supply, while the opposite end was sealed using speed tape and the custom mount to ensure that all injection flow was directed through the drilled holes. This configuration provided a rapid, low-cost method for assessing basic mass-injection behavior following the discontinuation of the tri-nozzle concept.

4.3 Manifold Setup

A custom manifold was 3D printed using Polycarbonate (PC). PC was chosen because its soluble supports allow the internal channels to be cleared completely. To ensure airtightness, the exterior was coated in a thin epoxy layer.

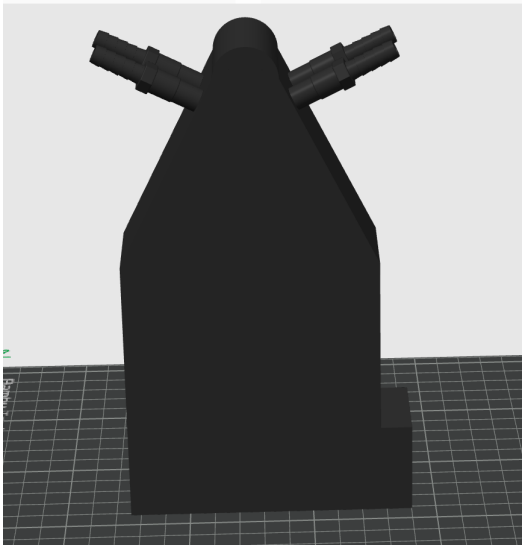


Figure 4.11: CAD model of the 3D-printed PC manifold used for secondary injection.

The initial manifold used four 1/8-in barbed fittings, later upgraded to 1/4-in fittings to reduce flow restriction. These fittings connected to the nozzle inlets via reinforced 200-psi-rated tubing.

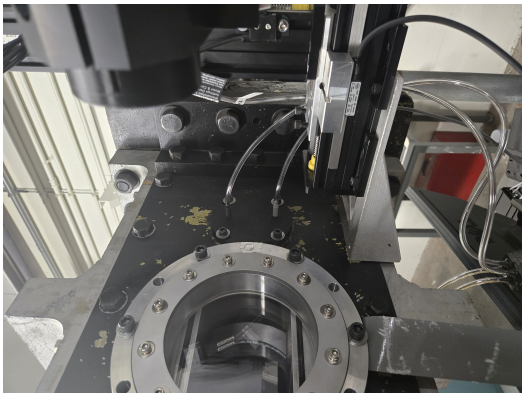


Figure 4.12: Experimental manifold setup with reinforced tubing.



Figure 4.13: Nitrogen-tank injection setup capable of supplying 120–200 psi through the manifold.

Air entrainment was insufficient to unstart the tunnel, so an air com-

pressor was added (75 psi). When that also failed, a nitrogen tank was used (125–200 psi).

4.4 Schlieren Camera Setup



Figure 4.14: The actual schlieren camera used in the experiment

A Schlieren system was integrated to visualize shock motion and flow separation. Schlieren imaging allowed direct observation of density gradients in the test section. The pressure regulator operator had direct visual access to the Schlieren screen, enabling real-time adjustment of injection pressure.

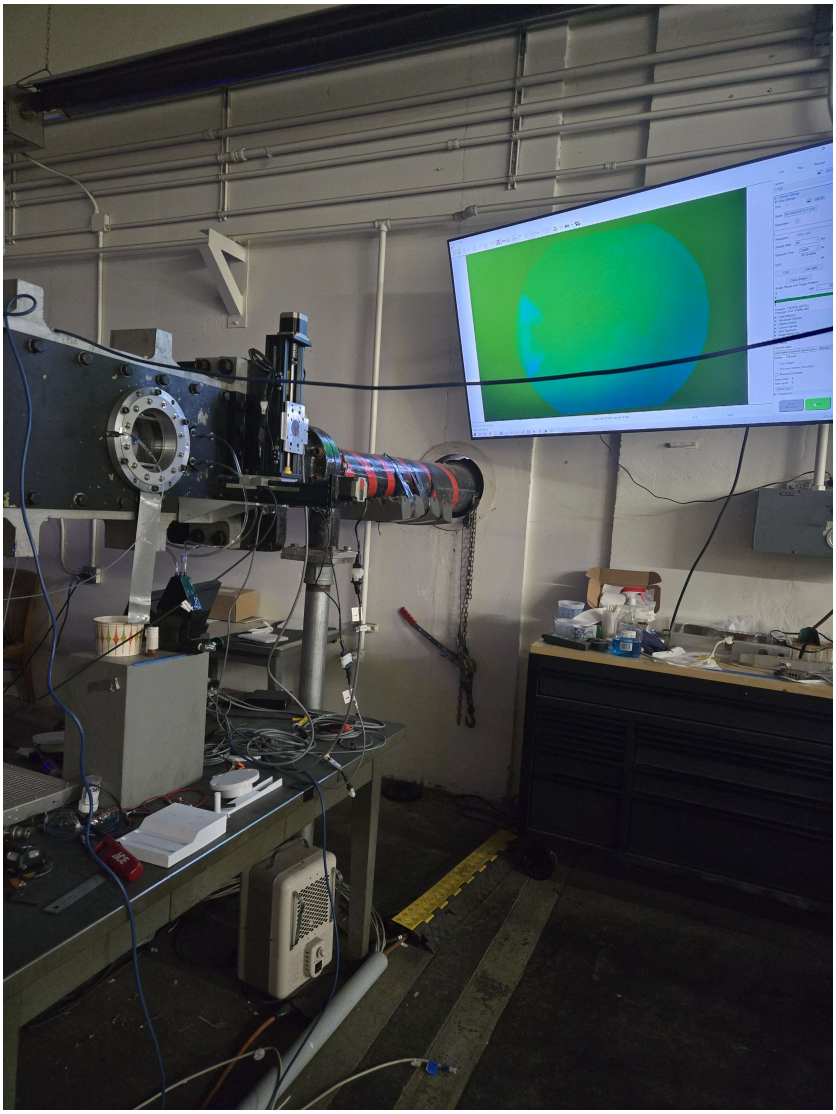


Figure 4.15: Schlieren system integrated into the Mach 4 wind tunnel.

4.5 Initial Schlieren Imaging Results

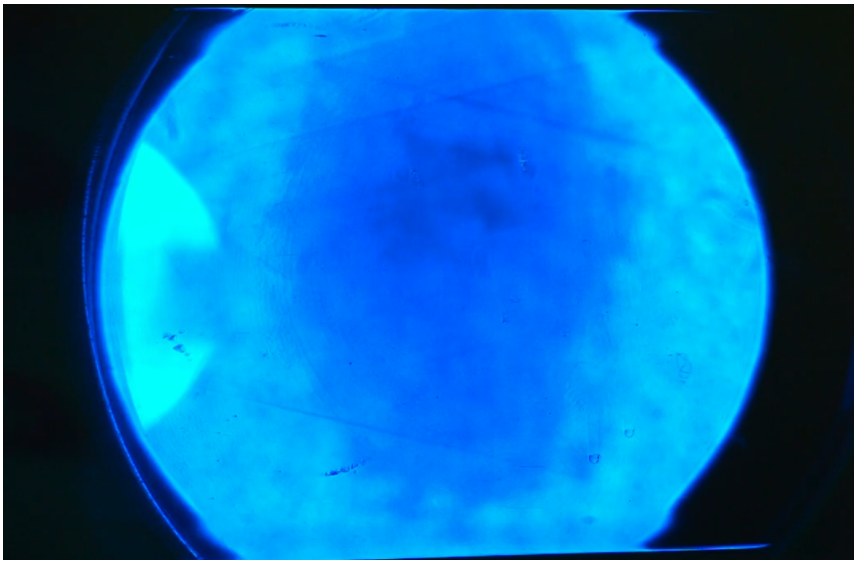


Figure 4.16: Sample Schlieren frame extracted during mass injection using the metal nozzle insert.

Initial Schlieren imaging was performed using the sharp, bladed metal nozzles shown in Figure 4.16, which represent the earliest prototypes developed for secondary mass injection. These nozzles were designed to introduce a localized disturbance into the flow while minimizing overall geometric blockage.

Despite increasing the injection pressure incrementally from 50 to 125 psi, none of the tests resulted in a global un-start of the tunnel. Schlieren visualization revealed the formation of localized compression waves and regions of limited flow reversal near the injector; however, the primary supersonic core flow remained intact throughout the test duration, as shown in



Figure 4.17: Bladed metal nozzle used for mass injection during early testing.

Figure 4.16. No sustained upstream shock propagation was observed.

These results indicate that the short, bladed nozzle configuration was insufficient to generate the level of geometric blockage or mass-flow disturbance required to induce un-start under Mach 4 operating conditions. Consequently, the nozzle geometry was redesigned to extend beyond the mounting region into the Schlieren window, allowing direct visualization of injection-induced flow disturbances. Following continued structural and integration challenges, the design was further simplified to the current metal pipe configuration.

Chapter 5

Results

5.1 CFD and Experimental Results for Metal Pipe Injection Geometry

The simulated results of the simplified metal pipe injection concept are shown in Figures 5.1 and 5.2, corresponding to pipe diameters of 0.6 in and 0.4 in located at the second throat of the Mach 4 wind tunnel. The primary objective of these simulations was to identify a pipe diameter small enough to avoid disrupting tunnel startup while still allowing secondary mass injection. However, both configurations produced a full un-start event in the simulations. In each case, the presence of the pipe introduced sufficient geometric blockage to generate a strong shock system that propagated upstream, resulting in collapse of the supersonic core flow. Although the 0.4 in diameter

pipe reduced the overall blockage relative to the 0.6 in case, the reduction was insufficient to preserve a fully started tunnel condition, indicating that even modest intrusions at the second throat are highly sensitive under Mach 4 operation. Smaller diameters were not evaluated numerically, as commercially available metal piping is not manufactured below 0.4 in diameter, making such configurations impractical for experimental implementation.

These simulations were conducted in two dimensions, which are known to over-predict blockage sensitivity relative to three-dimensional flow due to the absence of lateral flow relief. Nevertheless, the results demonstrate that the tunnel startup margin is extremely sensitive to blockage at the second throat and that even minimal pipe intrusions can trigger un-start in a two-dimensional configuration.

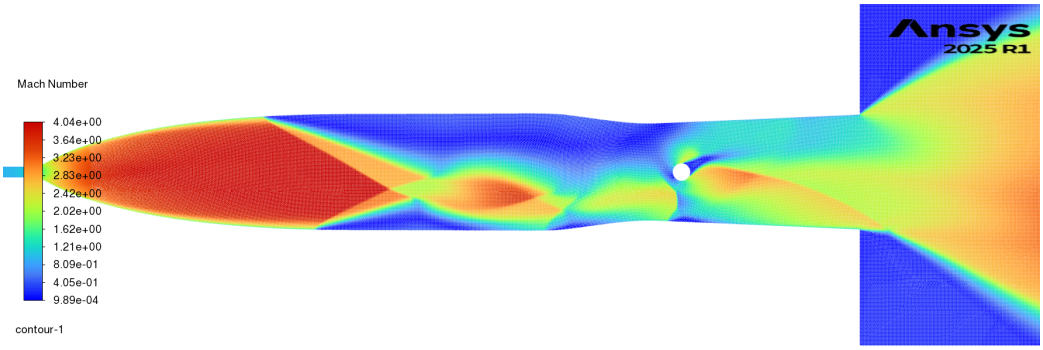


Figure 5.1: Ansys Fluent simulation of the tunnel with a 0.6 in diameter hole at the second throat.

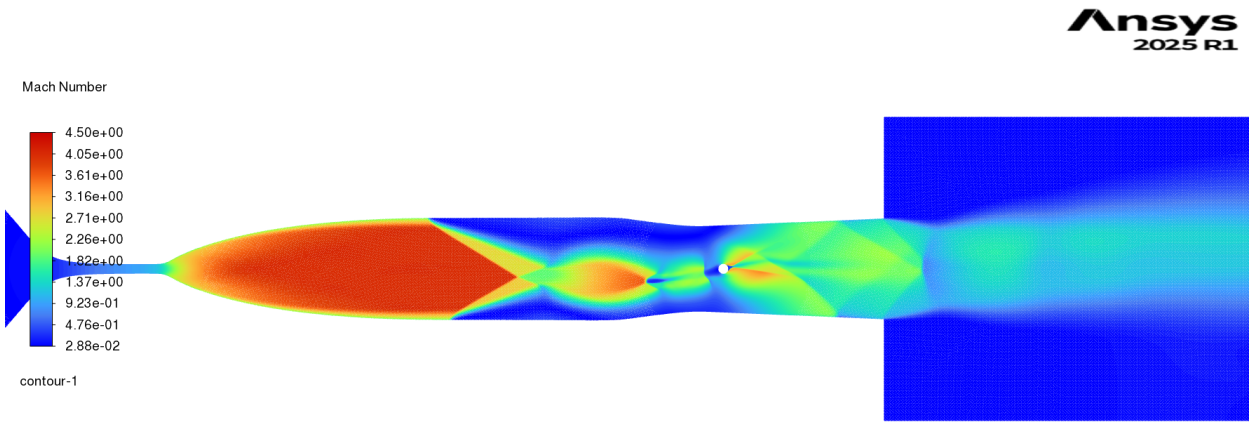


Figure 5.2: Ansys Fluent simulation of the tunnel with a 0.4 in diameter hole at the second throat.

5.1.1 Experimental Schlieren Imaging Results

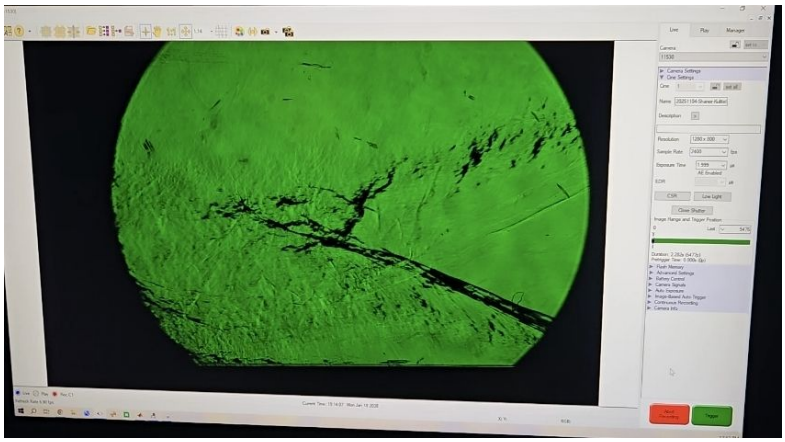


Figure 5.3: Live Schlieren image captured during tunnel operation with a 0.66 in diameter pipe installed and no secondary mass injection.

Schlieren imaging was used to qualitatively validate the CFD predictions for the simplified metal pipe configurations. Validation runs were conducted using pipe diameters similar to those evaluated numerically and operated without secondary mass injection. In both cases, distinct compression structures were observed within the Schlieren window, indicating the presence of strong shock–flow interactions induced by the geometric blockage of the pipe.

Consistent with the simulations, the experimental images show the formation of a localized shock structure in the vicinity of the test-section window rather than a classical shock diamond pattern. In the CFD results, this feature appears as a localized shock cell formed by interacting oblique shocks upstream of the blockage. While the precise axial location of the shock cell differs between simulation and experiment, the leading edge of the structure is clearly visible in both datasets, providing qualitative agreement in overall flow behavior.

As shown in Figures 5.3 and 5.2, the shock structure associated with the 0.66 in diameter pipe exhibits a relatively diffuse and unsteady shape, with the shock front appearing weakly defined and exhibiting noticeable variation during the run. In contrast, the 0.54 in diameter pipe produced a more sharply defined and stable shock structure that maintained its shape and position over time.

Chapter 6

Discussion

The combined CFD and experimental campaign yielded important insights into Mach 4 un-start behavior in the Naval Postgraduate School (NPS) wind tunnel, even though a complete un-start was not achieved experimentally. The discrepancy between simulation and physical testing highlights the inherent difficulty of reproducing injection-driven un-start in a facility where geometric constraints, structural survivability, and operational limits restrict the achievable disturbance to the supersonic core flow.

CFD predictions consistently indicated that mass injection through the tri-nozzle configuration was capable of producing a full un-start when a sufficient blockage ratio and injection pressure were applied. After correcting the outlet boundary conditions, the numerical model reliably generated a near-normal shock in the test section that propagated upstream and choked

the inlet. These results demonstrated that injection-induced un-start was physically feasible in principle and provided confidence in the underlying modeling methodology.

In contrast, none of the experimental attempts—including PLA, polycarbonate, ULTEM, and metal-based nozzle iterations—were able to generate a global un-start. Schlieren imaging confirmed localized disturbances, compression waves, and partial flow reversal near the injector, but the central supersonic core remained stable for all tested configurations. Several factors contributed to this outcome.

First, structural survivability of the injectors was a major limitation. Even the ULTEM nozzle, reinforced with epoxy, experienced severe vibration during Mach 4 operation and did not remain intact long enough to deliver the mass-flow levels indicated by CFD. These premature structural failures prevented the injector from providing sustained or high-pressure flow into the core stream. Second, the practical injection pressure used in testing (approximately 125–200 psi) was significantly lower than the effective mass-flow rates modeled numerically. Additional flow restrictions from the manifold, tubing, and nozzle geometry further reduced actual injection, diminishing the blockage ratio required to trigger un-start.

The government shutdown had a substantial impact on the project as well. All NPS spending authority was suspended, preventing the purchase of improved hardware such as metal additively manufactured injectors, up-

graded fittings, and additional argon required for metal printing. This interruption removed approximately 1.5 months of scheduled tunnel access and halted fabrication progress during a critical phase of the study. As a result, the experimental portion was conducted using only existing, pre-shutdown materials, limiting the ability to refine or upgrade the injection system.

Despite the inability to experimentally un-start the tunnel, the campaign successfully validated multiple aspects of the methodology. The CFD startup model was confirmed to be accurate, Schlieren imaging verified that disturbances formed in the predicted regions, and injector failure modes revealed the structural demands imposed by Mach 4 flow. These results provide a clear roadmap for future work: stronger metal injectors, improved manifold design, and higher-pressure regulated injection are all necessary to achieve the disturbance magnitudes predicted by CFD.

In summary, while a full un-start was not obtained experimentally within the constraints of this testing window, the combined numerical and experimental effort demonstrated the feasibility of injection-driven un-start and provided critical information for future experimentation once funding and facility operations resume.

Chapter 7

Application of Aerospace Engineering Science and Design Constraints

This project integrates core aerospace engineering sciences including aerodynamics, propulsion, flight mechanics, structural mechanics, and advanced materials to perform an in depth investigation of Mach 4 unstart dynamics in a supersonic wind tunnel. The work meets the ABET requirement of applying advanced engineering principles while addressing economic, environmental, social, political, ethical, health and safety, manufacturability, and sustainability constraints. The following sections summarize how each discipline and constraint guided the design, simulation, and experimentation

performed throughout this study.

7.1 Application of Aerospace Engineering

7.1.1 Aerodynamics and High Speed Flow Physics

Supersonic and hypersonic aerodynamics formed the core of this investigation. Computational fluid dynamics simulations were used to model shock wave formation, boundary layer growth, and shock boundary layer interaction under Mach 4 conditions. These analyses enabled identification of unstart mechanisms, prediction of shock motion during mass injection, and quantification of the pressure ratios required to disrupt the supersonic core flow. The aerodynamic loads derived from these simulations exceeded 16 kN on certain geometries, directly influencing material selection and nozzle survivability.

7.1.2 Propulsion and Inlet Dynamics

Although this study focuses on a wind tunnel rather than a flying vehicle, the physics of unstart remain identical to those that occur in scramjet inlets. The mass injection strategy reflects propulsion concepts such as backpressure rise, flow choking, isolator stability, and the Kantrowitz limit. The injection flow rates of 0.05 to 0.07 kilograms per second were selected using compressible flow equations and validated using momentum based analysis within the

computational models.

7.1.3 Flight Mechanics and Flow Stability

The motion of shocks in the test section was treated similarly to inlet unstart events observed during hypersonic flight. Flow oscillations, shock excursions, and local flow reversal revealed stability characteristics consistent with air breathing hypersonic systems. The Schlieren system enabled real time assessment of flow stability limits and overall unsteady behavior.

7.1.4 Aerospace Structures and Materials

The design and failure analysis of the tri nozzle injector required structural analysis under extreme aerodynamic loading. Material selection progressed from PLA to polycarbonate to ULTEM, and eventually to metal additive manufacturing. Performance was evaluated in terms of tensile strength, fatigue resistance, thermal softening, and vibrational stability. The catastrophic failures observed during testing validated the structural predictions and guided design refinement.

7.1.5 Manufacturability and Additive Manufacturing Science

Additive manufacturing processes including fused deposition modeling with polycarbonate and ULTEM, and later laser powder bed fusion metals, were

used to achieve complex internal channels required for controlled mass injection. Manufacturing constraints influenced channel geometry, wall thickness, print orientation, and post processing strategy. Vacuum oven drying, soluble supports, and tool access considerations were essential engineering factors to ensure successful fabrication.

7.2 Incorporation of Engineering Design Constraints

7.2.1 Economic Considerations

The choice of prototype materials, printing platforms, and nozzle geometries was strongly influenced by cost.

- Consumer grade prints allowed low cost iteration before committing to expensive ULTEM or metal fabrication.
- ULTEM printing on the Stratasys F900 and metal powder bed fusion introduced significant material and machine run time expenses.
- Powder procurement for metal printing requires an estimated minimum of ten thousand dollars, in addition to multiple tanks of argon, making cost a central design driver.

Government shutdown delays also influenced the economic timeline by restricting access to funding and test scheduling.

7.2.2 Environmental and Sustainability Constraints

The project minimized waste by relying on additive manufacturing, which produces significantly less scrap material compared to machining. Multi use polymer prototypes were produced only when necessary to reduce unused material. Additive manufacturing eliminates the need for cutting fluids, reducing environmental contamination. Nitrogen was selected as the injection gas because it is abundant, non toxic, and environmentally neutral.

7.2.3 Social and Political Constraints

Research conducted at the Naval Postgraduate School is influenced by institutional policies, facility access rules, and laboratory safety oversight. Political factors also affected the timeline, as a federal government shutdown prevented critical purchases and delayed testing for approximately one and a half months.

7.2.4 Ethical and Professional Responsibilities

All testing followed ethical engineering practice:

- Nozzle designs were validated through computational analysis and structural review before physical testing to avoid unsafe test configurations.
- Only materials capable of safe operation under Mach 4 loads were cleared for use inside the tunnel.

- Operators viewed the Schlieren screen from behind protective barriers, and injection tests were performed gradually to avoid sudden pressure spikes.

The design philosophy prioritized the safety of personnel, the integrity of the facility, and responsible use of laboratory resources.

7.2.5 Health and Safety Constraints

Mach 4 blowdown tunnels present significant safety concerns, including:

- High pressure nitrogen injection,
- High speed debris risk from nozzle failure,
- Exposure to fine metal powder during manufacturing,
- Elevated temperatures during polymer printing and part drying.

Risk mitigation included personal protective equipment, blast shielding, controlled pressure ramp procedures, and adherence to Naval Postgraduate School laboratory safety standards.

7.2.6 Manufacturability Constraints

Designs were constrained by the capabilities of each fabrication platform:

- Thin channels required soluble supports for polycarbonate or open back access for ULTEM.

- Overhang limits dictated nozzle orientation during printing.
- Metal additive manufacturing required support structures that could be removed mechanically without damaging functional regions.

These constraints resulted in several geometric iterations before arriving at a manufacturable configuration.

7.2.7 Sustainability Considerations

Sustainability was addressed through:

- Reducing waste via rapid low cost iterative prints,
- Selecting durable materials to avoid reprinting,
- Reusing metal hardware whenever possible,
- Avoiding hazardous chemicals during post processing.

The design approach emphasized long term resource efficiency and responsible use of materials.

7.3 Summary

This project demonstrates broad application of aerospace engineering science and responsible design constraints to the study of Mach 4 unstart. Aerodynamics, propulsion, structural mechanics, materials science, and manufacturability considerations were integrated into a complete system level in-

vestigation supported by computational modeling and experimental testing. Economic, environmental, social, political, ethical, safety, and sustainability constraints shaped every major decision in the design and testing process. The result is a technically rigorous and responsibly executed study that aligns with current expectations for modern aerospace engineering research.

Chapter 8

Conclusions and Future Work

This study investigated Mach 4 un-start dynamics in the Naval Postgraduate School (NPS) supersonic wind tunnel through a combined computational and experimental approach. High-fidelity CFD simulations demonstrated that a fixed-position mass-injection system was capable of generating a full un-start when an adequate blockage ratio and injection pressure were applied. The numerical predictions showed the formation of a near-normal shock in the test section, followed by upstream shock propagation and a complete breakdown of supersonic inlet flow. These results established a clear theoretical foundation for an injection-driven un-start mechanism.

The experimental phase, while informed directly by the CFD results, did not produce a global un-start. Multiple injector prototypes—ranging from PLA and polycarbonate to ULTEM and metal configurations—were

tested, but each design encountered structural or operational limitations. Severe vibration loads within the Mach 4 environment caused early structural failures, preventing the injectors from sustaining the mass-flow conditions required to match the CFD-predicted un-start threshold. Additionally, practical limits on injection pressure (approximately 125–200 psi) and flow restriction within the manifold system significantly reduced the achievable injection mass flow during testing.

Operational constraints further impacted the experimental campaign. A federal government shutdown halted all Naval Postgraduate School purchasing and fabrication activities, eliminating approximately 1.5 months of available wind tunnel time and preventing the production of improved metal injectors and upgraded injection hardware. As a result, testing proceeded with only the components that were fabricated prior to the shutdown, limiting opportunities for iterative refinement.

Despite these challenges, the research achieved several important outcomes. The CFD methodology was validated for Mach 4 startup behavior, injector-induced disturbances were visualized using Schlieren imaging, and the structural limitations of thermoplastic injectors under extreme aerodynamic loading were identified. Together, these findings provide a clear and actionable path for future un-start testing when funding and facility access are restored.

In conclusion, while a full injection-driven un-start was not achieved

experimentally, the work presented here establishes a robust computational baseline, defines the structural and operational requirements for successful un-start induction, and contributes new insights into the behavior of injection-triggered disturbances in a Mach 4 wind tunnel. With strengthened injection hardware and higher-pressure mass-flow capability, the methodology developed in this study remains a viable approach for future un-start investigations in hypersonic inlet research.

Bibliography

[1] Zha, G.-C., Knight, D. D., and Smith, D., "Numerical Investigations of HSCT Inlet Unstart Transient at Angle of Attack," *34th AIAA/ASME/SAE/ASEE Joint Propulsion Conference*, No. AIAA Paper 98-3583, Cleveland, OH, July 13-15 1998.

[2] Xu, S., Wang, Y., Wang, Z., Fan, X., and Xiong, B., "Experimental Investigations of Hypersonic Inlet Unstart/Restart Process and Hysteresis Phenomenon Caused by Angle of Attack," *Aerospace Science and Technology*, Vol. 126, 2022, pp. 107621.

[3] Lee, J. and Kang, S. H., "Numerical study on the start and unstart phenomena in a scramjet inlet-isolator model," *Plos one*, Vol. 14, No. 11, 2019, pp. e0224994.

[4] Laurie, A. M., Catherine, B., Griffin, C., and Robert, S., "Overview with results and lessons learned of the X-43 A Mach 10 flight," *AIAA/CIRA 13th Int. Space Planes and Hypersonics Systems and Technologies Conf., American Institute of Aeronautics and Astronautics, Reston, VA*, 2005.

[5] Wall, M., "Air Force's X-51A Hypersonic Scramjet Makes Record-Breaking Final Flight," *Space. com*, Vol. 3, 2013.

[6] Rosenberg, Z., "Second X-51 hypersonic flight ends prematurely," *Flight International. Flightglobal*, Vol. 15, 2011.

[7] Do, H., Im, S.-k., Mungal, M., and Cappelli, M., "Unstart of a Supersonic Model Inlet/Isolator Flow Induced by Mass Injection," *49th AIAA Aerospace Sciences Meeting including the New Horizons Forum and Aerospace Exposition*, 2011, p. 68.

[8] Trefny, C. J., "CFD Simulation of an Inward-Turning Supersonic Inlet Unstart at Flight Mach Number 1.7," *AIAA Propulsion and Energy 2020 Forum*, 2020, p. 3771.

[9] Mushtaq, N. and Gaetani, P., "Understanding and modeling unstarting phenomena in a supersonic inlet cascade," *Physics of Fluids*, Vol. 35, No. 10, 2023.

[10] Yu, K., Xu, J., Li, R., Liu, S., and Zhang, X., "Experimental exploration of inlet start process in continuously variable Mach number wind tunnel," *Aerospace Science and Technology*, Vol. 79, 2018, pp. 75–84.

[11] Nikaido, B. and Hobson, G. V., "RANS Predictions of Inlet/Isolator Unstart at Mach 4," *AIAA SCITECH 2025 Forum*, 2025, p. 0335.

[12] Plum, M., Dawe, G. F., Hobson, G. V., Nikaido, B., and Smith, W., "Flow Characterization of the NPS SupersonicWind Tunnel," *AIAA*

AVIATION FORUM AND ASCEND 2024, 2024, p. 4200.

[13] Redding, J., Cavanaugh, E., Bravo, L., Murugan, M., and Narayanaswamy, V., "High-Fidelity Simulations of Unstart Phenomena in a Scramjet Inlet Due to Angle of Attack," *arXiv preprint arXiv:2405.17671*, 2024.

[14] Zahrolayali, N., Saad, M. R., Idris, A. C., and Rahman, M. R. A., "Assessing the Performance of Hypersonic Inlets by Applying a Heat Source with the Throttling Effect," *Aerospace*, Vol. 9, No. 8, 2022, pp. 449.

[15] Li, T.-f., Ding, R.-h., Wang, W.-x., and Xie, W.-z., "Comparison of the unstart/restart processes of a two-dimensional twin-duct supersonic inlet induced by the plug throttling and thermal choking at the sideslip state," *Aerospace Science and Technology*, Vol. 142, 2023, pp. 108667.